

<b>Title</b>	Optical emission of strained direct-band-gap Ge quantum well embedded inside InGaAs alloy layers
<b>Author(s)</b>	Pavarelli, Nicola; Ochalski, Tomasz J.; Murphy-Armando, Felipe; Huo, Y.; Schmidt, Michael; Huyet, Guillaume; Harris, J. S.
<b>Publication date</b>	2013-04-25
<b>Original citation</b>	Pavarelli, N., Ochalski, T. J., Murphy-Armando, F., Huo, Y., Schmidt, M., Huyet, G. & Harris, J. S. (2013) 'Optical Emission of a Strained Direct-Band-Gap Ge Quantum Well Embedded Inside InGaAs Alloy Layers', Physical Review Letters, 110, 177404. <a href="http://dx.doi.org/10.1103/PhysRevLett.110.177404">http://dx.doi.org/10.1103/PhysRevLett.110.177404</a>
<b>Type of publication</b>	Article (peer-reviewed)
<b>Link to publisher's version</b>	<a href="http://link.aps.org/doi/10.1103/PhysRevLett.110.177404">http://link.aps.org/doi/10.1103/PhysRevLett.110.177404</a> <a href="http://dx.doi.org/10.1103/PhysRevLett.110.177404">http://dx.doi.org/10.1103/PhysRevLett.110.177404</a> Access to the full text of the published version may require a subscription.
<b>Rights</b>	© 2013 American Physical Society
<b>Item downloaded from</b>	<a href="http://hdl.handle.net/10468/2602">http://hdl.handle.net/10468/2602</a>

Downloaded on 2017-10-31T05:46:04Z

# Optical Emission of a Strained Direct-Band-Gap Ge Quantum Well Embedded Inside InGaAs Alloy Layers

N. Pavarelli,<sup>1,2</sup> T. J. Ochalski,<sup>1,2,\*</sup> F. Murphy-Armando,<sup>1</sup> Y. Huo,<sup>3</sup> M. Schmidt,<sup>1</sup> G. Huyet,<sup>1,2</sup> and J. S. Harris<sup>3</sup>

<sup>1</sup>Tyndall National Institute, University College Cork, Lee Maltings, Cork, Ireland

<sup>2</sup>Centre for Advanced Photonics and Process Analysis, Cork Institute of Technology, Cork, Ireland

<sup>3</sup>Electrical Engineering, Stanford University, Stanford, California 94305, USA

(Received 17 October 2012; published 25 April 2013)

We studied the optical properties of a strain-induced direct-band-gap Ge quantum well embedded in InGaAs. We showed that the band offsets depend on the electronegativity of the layer in contact with Ge, leading to different types of optical transitions in the heterostructure. When group-V atoms compose the interfaces, only electrons are confined in Ge, whereas both carriers are confined when the interface consists of group-III atoms. The different carrier confinement results in different emission dynamics behavior. This study provides a solution to obtain efficient light emission from Ge.

DOI: [10.1103/PhysRevLett.110.177404](https://doi.org/10.1103/PhysRevLett.110.177404)

PACS numbers: 78.67.De, 73.20.-r, 78.47.-p, 78.55.Ap

Ultrafast data transfer between and within microchips via high-speed optical interconnects represents an encouraging way forward for future progress in computer technology [1]. The advantages of implementing photonic devices made of silicon and germanium on integrated circuits have recently attracted much attention due to the possibility to integrate electronic and optical components on the same chip. Germanium is considered a promising material not only for the realization of high-performance photodetectors fully integrated on receiver chips [2], but also as an efficient on-chip light emitting source [3].

Emission from Ge, an indirect-band-gap semiconductor, was originally achieved by following a band-gap engineering strategy based on the combination of tensile strain and *n*-type doping in bulk Ge grown on Si [4,5]. This successful method led to the realization of light emitting sources [6–8] and optically pumped lasers [9] operating at 1.55  $\mu\text{m}$ . Similarly, direct-band-gap photoluminescence (PL) was obtained from other tensile-strained *n*-type Ge structures, where the strain was applied to the material using external mechanical methods [10–13].

An alternative approach employs highly tensile-strained Ge, where a sufficient amount of strain, calculated to be between 1.7% and 1.9% [14–16], pushes the  $\Gamma$  valley minimum below the *L* valley minimum. The growth of highly strained Ge requires III-V matrixes. To date, a few high-quality Ge on  $\text{In}_x\text{Ga}_{1-x}\text{As}$  structures have been reported [17–19], but without the desired level of strain to obtain direct-band-gap PL from undoped Ge. Although the fabrication of such structures is quite difficult, Huo *et al.* [20] recently demonstrated the growth of  $\sim 2.3\%$  tensile-strained Ge layers embedded in  $\text{In}_{0.40}\text{Ga}_{0.60}\text{As}$ , and confirmed their direct-band-gap nature by a strong emission from the intrinsic Ge.

In this work, the optical properties and the calculated band structure of a  $\sim 2\%$  in-plane biaxial tensile-strained 6 nm Ge quantum well (QW) embedded in two relaxed  $\text{In}_{0.30}\text{Ga}_{0.70}\text{As}$

barrier layers are reported. The schematic of the structure and two cross-section transmission electron microscopy (TEM) images are shown in Fig. 1. The growth conditions and the material characterization can be found in Ref. [20].

The theoretical understanding of the band structure is essential to predict the radiative recombination channels of this material. The conduction and the valence band offsets (CBO and VBO) between  $\text{In}_{0.30}\text{Ga}_{0.70}\text{As}$  and Ge were calculated using density functional theory in the local density approximation, employing a similar method to the average potential of Ref. [21]. Unlike [21], the atomic bonds at the interface were considered explicitly, rather than an interface made up of the average mixture of the bonded atoms. The average potentials were calculated across the interfaces for the two most extreme stoichiometries:  $\frac{1}{2}\text{Ge}-\frac{1}{2}\text{As}$  and  $\frac{1}{2}\text{Ge}-\frac{1}{2}(\text{In}_{0.30}\text{Ga}_{0.70})$ , treating the group-III atomic potential as an average of 30% In and 70% Ga within the virtual crystal approximation. The supercells consisted of 12 Ge and 12 III-V atoms.

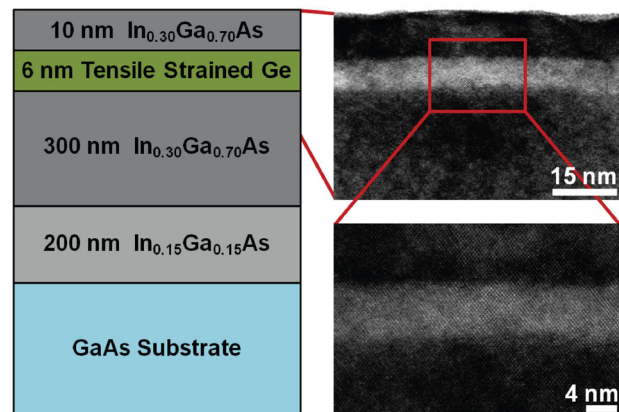


FIG. 1 (color online). Schematic and cross-section TEM images of the  $\sim 2\%$  in-plane biaxial tensile-strained Ge QW embedded in relaxed  $\text{In}_{0.30}\text{Ga}_{0.70}\text{As}$  layers.

The average potential in the Ge and III-V regions, and the resulting band offsets, were calculated as in Ref. [21]. The offsets for intermediate stoichiometries were interpolated between the two extremes. The band gaps and the effect of the quantum confinement were calculated using the Green-Coulomb (GW) approximation [22] and the  $\mathbf{k} \cdot \mathbf{p}$  method [23], respectively.

When bulk Ge is grown between two barriers of fully relaxed  $\text{In}_{0.30}\text{Ga}_{0.70}\text{As}$ , its lattice is  $\sim 2\%$  tensile strained in the plane and relaxed along the growth direction  $z$ . This amount of strain changes the minimum of the conduction band from  $L$  to  $\Gamma$ , and splits the light holes (LH) and heavy holes (HH) in the valence band. The LH and HH bands are shifted higher and lower in energy, respectively, and the 2% tensile-strained Ge band gap is 0.32 eV with LH and 0.64 eV with HH. The LH band has a  $p_z$  orbital character; hence, the photons generated by the recombination between the LH and the electrons in  $\Gamma$  ( $e - \Gamma$ ) are emitted in the plane of the structure and are likely not detected, since the PL is collected from the top of the sample. In contrast, the radiative recombination between HH and  $e - \Gamma$  is emitted along  $z$  and represents the main component of the emission measured in the experiments [24].

The (100) planes of atoms in III-V zinc-blende crystals are polar, as alternate planes are ideally formed only by group-III or group-V atoms. For group-IV diamond crystals the planes contain just one type of atom and are equivalent. At the interface between the two crystals the planes retain their properties, but the stoichiometry changes. For this structure, the two extreme situations are those where the  $\text{In}_{0.30}\text{Ga}_{0.70}\text{As}$  terminates at the Ge interface with a uniform layer containing exclusively either group-III or group-V atoms. Depending on these terminations, due to the difference in electronegativity between the constituent atomic species, dipoles of opposite sign can be created at the Ge-InGaAs interface. In terms of band structure, the electrostatic potential resulting from the large variation in the interface dipoles produces significant changes in the band offset between the  $\text{In}_{0.30}\text{Ga}_{0.70}\text{As}$  and Ge ([25] and cited therein). Since this interface can in principle have any stoichiometry, the band structure can assume all the possible configurations between the two aforementioned cases.

The optical transition energies of all possible radiative recombination channels, calculated as a function of the Ge-InGaAs interface stoichiometry  $[(\text{In}_{0.30}\text{Ga}_{0.70})_y\text{As}_{1-y}]$ , are presented in Fig. 2. For pure Ge-V bonds ( $y = 0$ ), the confinement occurs only in the conduction band, with the two confined electron states,  $E0$  and  $E1$ , 0.23 and 0.53 eV above the Ge conduction band edge, respectively. The band alignment is type-II and the emission is characterized by a ground state (GS) and an excited state (ES) both occurring between the electrons in the Ge QW and the holes in the  $\text{In}_{0.30}\text{Ga}_{0.70}\text{As}$  barriers. The interface band offsets linearly depend on the stoichiometry. When  $y$  increases, the CBO decreases, but the Ge band gap remains constant. This lifts the position of the confined electron levels, despite the

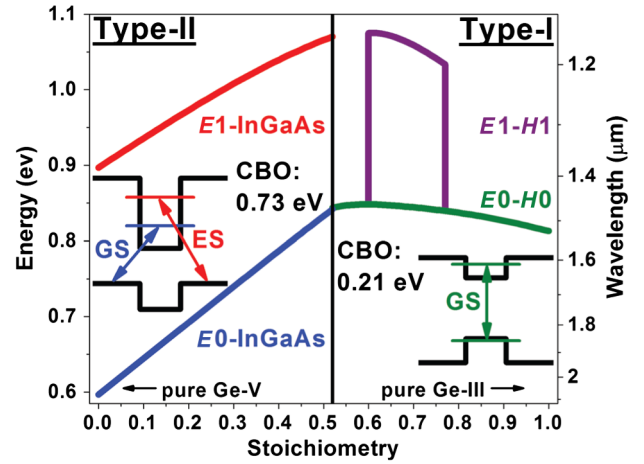


FIG. 2 (color online). Optical transition energies as a function of the Ge-InGaAs interface stoichiometry. The vertical black line represents the transition from type-II to type-I band alignment. The calculated band structure for pure Ge-V (Ge-III) bonds is depicted in the left-hand (right-hand) side inset. In both cases the arrows represent the possible radiative recombination channels.

progressive reduction of electron quantum confinement, resulting in an overall increase of optical transition energies for both GS and ES (blue  $E0$ -InGaAs and red  $E1$ -InGaAs lines, respectively, in Fig. 2).

At  $y = 0.52$  the VBO is zero, marking the transition between type-II and type-I band alignment (vertical line in Fig. 2). For  $y$  greater than 0.52, once the holes become sufficiently confined in the Ge QW, the radiative recombination is type-I and occurs between the lowest electron and hole levels ( $E0$  and  $H0$ , respectively). As  $y$  further increases, the reduction of electron quantum confinement, together with the rise of  $H0$ , causes the progressive decrease of the optical transition energy (green  $E0$ - $H0$  line in Fig. 2). At  $y = 0.60$  the Ge potential well in the valence band is deep enough to confine a second hole state ( $H1$ ), resulting in an additional radiative recombination channel (purple  $E1$ - $H1$  line in Fig. 2) occurring between  $E1$  and  $H1$ . For values of  $y$  higher than 0.77, the potential well in the conduction band becomes too shallow to confine more than one electron state, and the only possible optical transition is the  $E0$ - $H0$  GS. Finally, when the stoichiometry reaches the extreme case of pure Ge-III bonds ( $y = 1$ ), the GS emission exhibits the lowest energy (0.81 eV) for the type-I alignment.

This theoretical approach considers for simplicity a Ge QW embedded within two  $\text{In}_{0.30}\text{Ga}_{0.70}\text{As}$  layers where both interfaces have identical stoichiometry. However, in the case of mixed interfaces, the holes in the valence band are not confined in the QW since the InGaAs layers form a potential barrier only on one side of the Ge. Therefore the emission has a type-II character and occurs at 0.51 eV, a value well beyond the range of interest for this structure.

It is worth noting that for a 6 nm QW, since the  $\Gamma$  and  $L$  states are confined in finite wells with different potential barriers, the effect of the quantum confinement is not the same in each valley. Moreover, for  $\sim 2\%$  strain, the

electron effective mass in  $\Gamma$  is  $\sim 7$  times smaller than in  $L$ ; hence, the energy dispersion of the former valley is much sharper than that of the latter. This results in the confined GS in  $\Gamma$  lying  $\sim 90$  and  $\sim 30$  meV above the confined GS in  $L$  for  $y = 0$  and  $y = 1$ , respectively. Despite the fact that the band gap is not strictly direct, the photo-carrier density generated during the optical characterization is sufficient to produce PL, as previously observed in Ref. [24].

In reality, the Ge-InGaAs interface is not perfectly uniform and flat, but is likely characterized by atomic-height steps which separate terraces terminating with atoms of the same group. It is therefore plausible to have the formation of two different types of domains: group-V-bound Ge and group-III-bound Ge, giving rise to the presence of type-I and type-II optical transitions in spatially distinct areas of the same structure. The optical characterization was performed at 10 K via microphotoluminescence ( $\mu$ -PL) and micro-time-resolved PL ( $\mu$ -TRPL), as described in Ref. [26]. In both cases the laser was focused using a high numerical aperture objective on a spot of  $\sim 5$   $\mu\text{m}$  diameter on the sample surface. This spot size allowed the independent detection of type-I and type-II optical transitions in spatially distinct areas of the sample. However, since the majority of the measurements revealed the simultaneous presence of both emission features in a single spectrum, the average domain size should be smaller than the laser spot.

Figure 3(a) shows power-dependent PL results for the type-II group-V-bound Ge domains. The peak at 1.110 eV corresponds to the  $\text{In}_{0.30}\text{Ga}_{0.70}\text{As}$  band gap, while the two other peaks at lower energies originate from the radiative recombination occurring between the holes in the  $\text{In}_{0.30}\text{Ga}_{0.70}\text{As}$  barriers and either the  $E0$  (0.705 eV) or the  $E1$  (1.040 eV) electron levels in the Ge QW. The low-energy side of the spectrum was multiplied by 150 to account for the low detector sensitivity in this spectral region. Both GS and ES emissions exhibit a strong redshift with decreasing the excitation power, which can be explained in terms of Coulomb interactions between the differently confined carriers [27,28]. Under high-power excitation, the Coulomb potential modifies the energy bands and lifts the position of the confined electron levels, as schematically depicted in the inset in Fig. 3(a). Under low-power excitation, the carrier interactions are weak and the Coulomb potential does not significantly affect the energy bands. In these conditions the discrepancy between experiments and theory (evaluated at zero carrier density) is minimal, and from the ES peak measured at the lowest power density the average stoichiometry for these domains is approximately  $(\text{In}_{0.30}\text{Ga}_{0.70})_{0.2}\text{As}_{0.8}$ .

Further analysis can be performed by studying the behavior of the energy shift ( $\Delta E$ ) and the integrated PL intensity ( $I_{\text{PL}}$ ) of these emission features. Because of low detector sensitivity below 0.75 eV, the range of powers explored is different for each state. The GS and ES total shifts are  $\sim 25$  and  $\sim 60$  meV, respectively. Nevertheless, the two lines in Fig. 3(b) are parallel within experimental errors, indicating comparable peak position changes for a

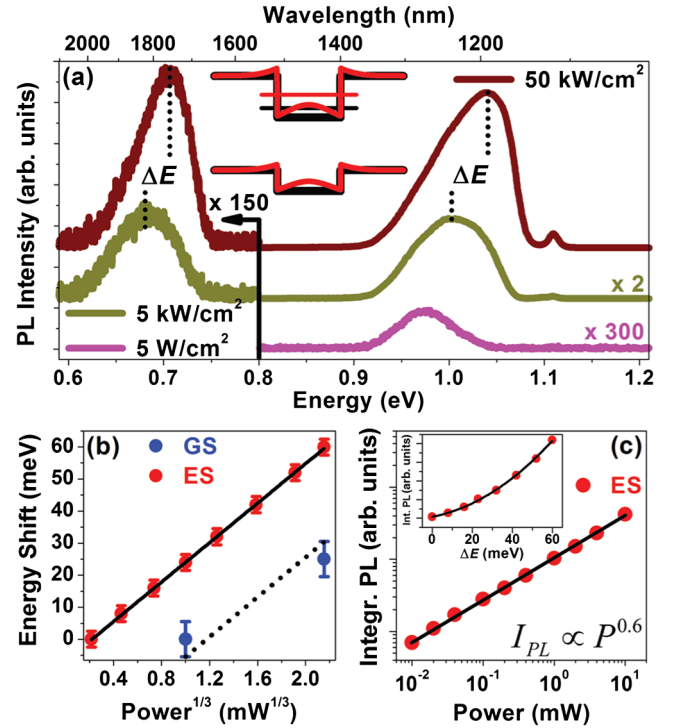


FIG. 3 (color online). Optical properties of the type-II group-V-bound Ge domains. (a) Power-dependent PL spectra. Band structure and energy level modifications due to the Coulomb interactions between the spatially separated carriers are schematically depicted in the inset. (b) PL peak shifts as a function of the third root of the power. (c) Power dependence of integrated PL intensity. The quadratic behaviour of  $I_{\text{PL}}$  as a function of  $\Delta E$  is depicted in the inset. Solid lines are the fits of the experimental data, while dotted lines are a guide for eyes.

given power variation for both states. Moreover, the linear dependence between the shift and the third root of the excitation power ( $P$ ) indicates a type-II band alignment for this emission [29,30].

Additionally, the exponent  $m$  in the formula  $I_{\text{PL}} \propto P^m$  provides information on the dominant mechanism responsible for the light emission in the material. For exciton recombination  $m \approx 1$ , while for free-carrier recombination  $m \approx 2$  [31,32]. The sublinear relation ( $m < 1$ ) between  $I_{\text{PL}}$  and  $P$  in Fig. 3(c) suggests the presence of a dominant loss mechanism inhibiting the PL, such as the presence of dislocations in the fully relaxed barriers, or may simply suggest reduced emission efficiency caused by the low wavefunction overlap between spatially separated carriers [33]. Moreover, the quadratic dependence between  $I_{\text{PL}}$  and  $\Delta E$ , depicted in the inset in Fig. 3(c), further confirms that these behaviors are due to dipole-dipole interactions occurring between the spatially separated carriers in type-II structures.

TRPL results are presented in Fig. 4 using a streak image. Because of the streak camera photocathode cutoff at 0.83 eV, one can detect only the  $\text{In}_{0.30}\text{Ga}_{0.70}\text{As}$  barrier emission feature and the type-II ES. For the latter, immediately after the laser pulse ( $t = 0$ ), the emission is blue-shifted to 1.060 eV. The radiative recombination then



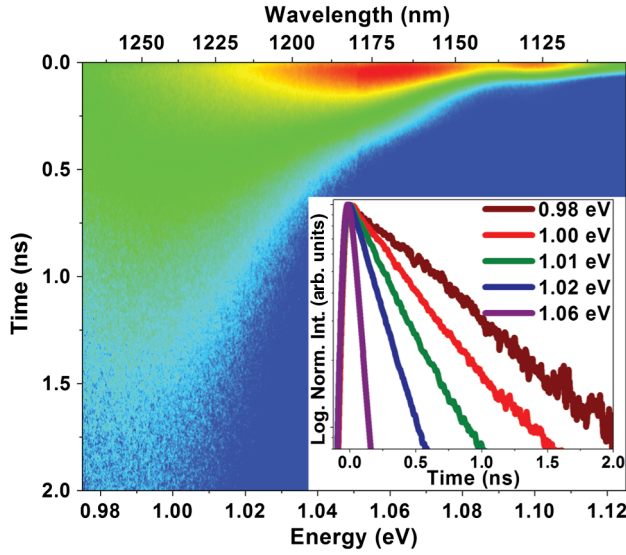


FIG. 4 (color online). Streak image (representing the logarithm of the emission intensity in color scale as a function of energy and time) of the type-II group-V-bound Ge domains. Decay traces extracted from the streak image at selected emission energies are depicted in the inset.

depletes the structure and the emission redshifts toward its zero-carrier position. This change of peak position is accompanied by a simultaneous change of carrier lifetime [34–36]. At  $t = 0$  the holes in the  $\text{In}_{0.30}\text{Ga}_{0.70}\text{As}$  are strongly attracted by the electrons confined in the Ge QW and the optical matrix element, proportional to the overlap between the constituent wave functions, is maximum. Therefore the associated carrier lifetimes are short. With elapsing time, the carrier density and the wave-function overlap decrease, the emission energy redshifts and the carrier lifetimes become longer.

Wavelength-dependent emission dynamics are presented in the inset in Fig. 4, where a comparison of decay traces confirms that the high-energy side of the spectrum exhibits faster dynamics than the low-energy side. Decay times corresponding to the selected energies were extracted by fitting each decay trace with a single exponential function, and range from 0.08 ns at 1.060 eV to 0.94 ns at 0.980 eV. Note that, due to the emission redshift, these fitted decay times are slightly shorter than the true decay times. Nevertheless, they provide a good estimate and the trend of increasing lifetime with decreasing carrier density is still valid.

Figure 5(a) shows power-dependent PL results for the type-I group-III-bound Ge domains. The emission feature observed at 0.835 eV originates from the radiative recombination between the  $E0$  and  $H0$  levels confined in the Ge QW. This peak does not exhibit any significant shift with decreasing power density, which is a straightforward consequence of the minimal effect of the Coulomb interactions on the type-I band alignment. The emission energy measured in the experiments agrees with the calculations if Ge domains characterized by the majority of Ge-InGa bonds

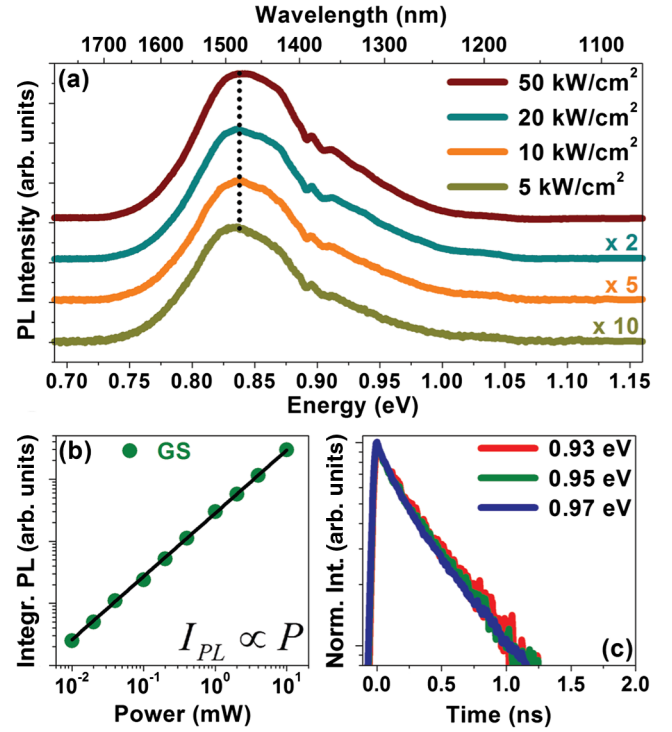


FIG. 5 (color online). Optical properties of the type-I group-III-bound Ge domains. (a) Power-dependent PL spectra. The dotted line is a guide for eyes. (b) Power dependence of integrated PL intensity. The solid line is the fit of the experimental data. (c) Decay traces at selected emission energies.

(80%–85%) are considered. Moreover, the linear dependence between  $I_{PL}$  and  $P$  in Fig. 5(b) suggests that the fundamental mechanism of radiative recombination for the group-III-bound Ge domains is exciton and not free-carrier recombination.

Finally, the emission dynamics are presented in Fig. 5(c). The decay traces for this type-I optical transition are energy independent. The decay times are obtained by fitting the decay traces with a single exponential function. The average value is 0.42 ns with a standard deviation comparable with the temporal resolution of the experiment (20 ps). This is consistent with the carrier lifetimes of conventional III-V type-I QWs [37], indicating good optical properties of the structure under investigation.

In conclusion, we have studied the optical properties of a direct-band-gap  $\sim 2\%$  tensile-strained Ge QW embedded in relaxed  $\text{In}_{0.30}\text{Ga}_{0.70}\text{As}$  layers. The optical characterization revealed the presence of type-I and type-II optical transitions in spatially distinct areas of the same structure. Calculations showed that the band structure changes with the Ge-InGaAs interface stoichiometry, ranging from a type-II alignment for pure Ge-As bonds to a type-I alignment for the opposite situation. In both cases, the theoretical optical transition energies agree with experiments, suggesting the formation of Ge domains with submicron dimensions where the stoichiometry is either predominantly group-V bound or predominantly group-III bound. Moreover, the optical characterization did not reveal

emission energies associated with intermediate stoichiometries, which may indicate that such Ge-InGaAs interfaces are not highly probable or chemically stable. The band structure of Ge embedded in III-V alloys can thus be tailored by controlling the termination of the barrier layers at the interface with the Ge ([38] and cited therein), leading to the realization of either type-I optical devices (emitters, modulators, amplifiers) or type-II high-performance tunneling field-effect transistors [39]. A significant advantage of this system is the possibility of designing structures where distinct areas have either type-I or type-II band alignment, offering the potential to achieve integrated circuits with complex optical and electronic functionalities coexisting on the same wafer.

This work was supported by Science Foundation Ireland (Grants No. 07/IN.1/I929, No. 07/IN.1/I1810, and No. 09/SIRG/I1621), Enterprise Ireland (Grant No. RE/2007/006) and the INSPIRE programme under the HEA PRTL Cycle 4, National Development Plan 2007-2013. F.M.-A. would like to acknowledge Stephen Fahy for stimulating discussions.

---

\*tomasz.ochalski@tyndall.ie

- [1] J. D. Meindl, *Comput. Sci. Eng.* **5**, 20 (2003).
- [2] J. Michel, L. Liu, and L. C. Kimerling, *Nat. Photonics* **4**, 527 (2010).
- [3] D. Liang and J. E. Bowers, *Nat. Photonics* **4**, 511 (2010).
- [4] Y. Ishikawa, K. Wada, D. D. Cannon, J. Liu, H.-C. Luan, and L. C. Kimerling, *Appl. Phys. Lett.* **82**, 2044 (2003).
- [5] J. Liu, X. Sun, D. Pan, X. Wang, L. C. Kimerling, T. L. Koch, and J. Michel, *Opt. Express* **15**, 11 272 (2007).
- [6] X. Sun, J. Liu, L. C. Kimerling, and J. Michel, *Opt. Lett.* **34**, 1198 (2009).
- [7] X. Sun, J. Liu, L. C. Kimerling, and J. Michel, *Appl. Phys. Lett.* **95**, 011911 (2009).
- [8] W. Hu, B. Cheng, C. Xue, H. Xue, S. Su, A. Bai, L. Luo, Y. Yu, and Q. Wang, *Appl. Phys. Lett.* **95**, 092102 (2009).
- [9] J. Liu, X. Sun, R. Camacho-Aguilera, L. C. Kimerling, and J. Michel, *Opt. Lett.* **35**, 679 (2010).
- [10] M. El Kurdi, H. Bertin, E. Martincic, M. de Kersauson, G. Fishman, S. Sauvage, A. Bosseboeuf, and P. Boucaud, *Appl. Phys. Lett.* **96**, 041909 (2010).
- [11] T.-H. Cheng, K.-L. Peng, C.-Y. Ko, C.-Y. Chen, H.-S. Lan, Y.-R. Wu, C. W. Liu, and H.-H. Tseng, *Appl. Phys. Lett.* **96**, 211108 (2010).
- [12] H.-S. Lan, S.-T. Chan, T.-H. Cheng, C.-Y. Chen, S.-R. Jan, and C. W. Liu, *Appl. Phys. Lett.* **98**, 101106 (2011).
- [13] D. Nam, D. Sukhdeo, S.-L. Cheng, A. Roy, K. C.-Y. Huang, M. Brongersma, Y. Nishi, and K. Saraswat, *Appl. Phys. Lett.* **100**, 131112 (2012).
- [14] C. G. Van de Walle, *Phys. Rev. B* **39**, 1871 (1989).
- [15] M. V. Fischetti and S. E. Laux, *J. Appl. Phys.* **80**, 2234 (1996).
- [16] M. El Kurdi, G. Fishman, S. Sauvage, and P. Boucaud, *J. Appl. Phys.* **107**, 013710 (2010).
- [17] Y. Bai, K. E. Lee, C. Cheng, M. L. Lee, and E. A. Fitzgerald, *J. Appl. Phys.* **104**, 084518 (2008).
- [18] Y. Hoshina, A. Yamada, and M. Konegai, *Jpn. J. Appl. Phys.* **48**, 111102 (2009).
- [19] R. Jakomin, M. de Kersauson, M. El Kurdi, L. Largeau, O. Mauguin, G. Beaudoin, S. Sauvage, R. Ossikovski, G. Ndong, M. Chaigneau, I. Sagnes, and P. Boucaud, *Appl. Phys. Lett.* **98**, 091901 (2011).
- [20] Y. Huo, H. Lin, R. Chen, M. Makarova, Y. Rong, M. Li, T. I. Kamins, J. Vuckovic, and J. S. Harris, *Appl. Phys. Lett.* **98**, 011111 (2011).
- [21] K. Kunc and R. M. Martin, *Phys. Rev. B* **24**, 3445 (1981).
- [22] M. S. Hybertsen and S. G. Louie, *Phys. Rev. B* **34**, 5390 (1986).
- [23] F. Murphy-Armando and S. Fahy, *J. Appl. Phys.* **109**, 113703 (2011).
- [24] J. R. Sanchez-Perez, C. Boztug, F. Chen, F. F. Sudradjat, D. M. Paskiewicz, R. B. Jacobson, M. G. Lagally, and R. Paiella, *Proc. Natl. Acad. Sci. U.S.A.* **108**, 18 893 (2011).
- [25] A. Munoz, N. Chetty, and R. M. Martin, *Phys. Rev. B* **41**, 2976 (1990).
- [26] N. Pavarelli, T. J. Ochalski, H. Y. Liu, K. Gradkowski, M. Schmidt, D. P. Williams, D. J. Mowbray, and G. Huyet, *Appl. Phys. Lett.* **101**, 231109 (2012).
- [27] F. Hatami, N. N. Ledentsov, M. Grundmann, J. Bohrer, F. Heinrichsdorff, M. Beer, D. Bimberg, S. S. Ruvimov, P. Werner, U. Gosele, J. Heydenreich, U. Richter, S. V. Ivanov, B. Ya. Meltser, P. S. Kop'ev, and Zh. I. Alferov, *Appl. Phys. Lett.* **67**, 656 (1995).
- [28] C.-K. Sun, G. Wang, J. E. Bowers, B. Brar, H.-R. Blank, H. Kroemer, and M. H. Pilkuhn, *Appl. Phys. Lett.* **68**, 1543 (1996).
- [29] N. N. Ledentsov, J. Bohrer, M. Beer, F. Heinrichsdorff, M. Grundmann, D. Bimberg, S. V. Ivanov, B. Ya. Meltser, S. V. Shaposhnikov, I. N. Yassievich, N. N. Faleev, P. S. Kop'ev, and Zh. I. Alferov, *Phys. Rev. B* **52**, 14 058 (1995).
- [30] F. Hatami, M. Grundmann, N. N. Ledentsov, F. Heinrichsdorff, R. Heitz, J. Bohrer, D. Bimberg, S. S. Ruvimov, P. Werner, V. M. Ustinov, P. S. Kop'ev, and Zh. I. Alferov, *Phys. Rev. B* **57**, 4635 (1998).
- [31] S. R. Jin, Y. L. Zheng, and A. Z. Li, *J. Appl. Phys.* **82**, 3870 (1997).
- [32] S. Martini, A. A. Quivy, A. Tabata, and J. R. Leite, *J. Appl. Phys.* **90**, 2280 (2001).
- [33] J. He, C. J. Reyner, B. L. Liang, K. Nunna, D. L. Huffaker, N. Pavarelli, K. Gradkowski, T. J. Ochalski, G. Huyet, V. G. Dorogan, Yu. I. Mazur, and G. J. Salamo, *Nano Lett.* **10**, 3052 (2010).
- [34] Y. D. Jang, T. J. Badcock, D. J. Mowbray, M. S. Skolnick, J. Park, H. Y. Liu, M. J. Steer, and M. Hopkinson, *Appl. Phys. Lett.* **92**, 251905 (2008).
- [35] J. Tatebayashi, B. L. Liang, R. B. Laghumavarapu, D. A. Bussian, H. Htoon, V. Klimov, G. Balakrishnan, L. R. Dawson, and D. L. Huffaker, *Nanotechnology* **19**, 295704 (2008).
- [36] K. Gradkowski, T. J. Ochalski, N. Pavarelli, H. Y. Liu, J. Tatebayashi, D. P. Williams, D. J. Mowbray, G. Huyet, and D. L. Huffaker, *Phys. Rev. B* **85**, 035432 (2012).
- [37] Th. Amand, X. Marie, B. Dareys, J. Barrau, M. Brousseau, D. J. Dunstan, J. Y. Emery, and L. Goldstein, *J. Appl. Phys.* **72**, 2077 (1992).
- [38] Y. Li, L. Lazzarini, L. J. Giling, and G. Salviati, *J. Appl. Phys.* **76**, 5748 (1994).
- [39] P. Guo, Y. Yang, Y. Cheng, G. Han, J. Pan, Ivana, Z. Zhang, H. Hu, Z. X. Shen, C. K. Chia, and Y.-C. Yeo, *J. Appl. Phys.* **113**, 094502 (2013).